Langmuir
Article
pubs.acs.org/Langmuir

How To Prepare and Stabilize Very Small Nanoemulsions

Thomas Delmas,[†,‡] Hélène Piraux,[‡] Anne-Claude Couffin,[*,†] Isabelle Texier,[*,†] Françoise Vinet,[†] Philippe Poulin,[§] Michael E. Cates,[⊥] and Jérôme Bibette[*,‡]

[†]*CEA-LETI, Campus MINATEC, Département des Technologies pour la Biologie et la Santé, 17 rue des Martyrs, F-38054 Grenoble, France,* [‡]*LCMD ESPCI, CNRS UMR 7612, 10 rue Vauquelin, 75005 Paris, France,* [§]*CRPP, Université Bordeaux, CNRS, Avenue Schweitzer 33600 Pessac, France, and* [⊥]*SUPA, School of Physics & Astronomy, University of Edinburgh, Edinburgh EH9 3JZ, Scotland*

Received October 20, 2010. Revised Manuscript Received December 17, 2010

Practical and theoretical considerations that apply when aiming to formulate by ultrasonication very small nanoemulsions (particle diameter up to 150 nm) with very high stability are presented and discussed. The droplet size evolution during sonication can be described by a monoexponential function of the sonication time, the characteristic time scale depending essentially on the applied power. A unique master curve is obtained when plotting the mean diameter size evolution as a function of sonication energy. We then show that Ostwald ripening remains the main destabilization mechanism whereas coalescence can be easily prevented due to the nanometric size of droplets. The incorporation of "trapped species" within the droplet interior is able to counteract Ostwald ripening, and this concept can be extended to the membrane compartment. We finally clarify that nanoemulsions are not thermodynamically stable systems, even in the case where their composition lies very close to the demixing line of a thermodynamically stable microemulsion domain. However, as exemplified in the present work, nanoemulsion systems can present very long-term kinetic stability.

Introduction

Among the different emulsions, nanoemulsions differ from common macro- or microscopic sized emulsions (droplet size $>1\ \mu$m) because they form almost transparent or translucent systems in which droplet sizes range from 20 to 200 nm.[1,2] (Note that nanoemulsions are also referred as miniemulsions, submicrometer emulsions, or ultrafine emulsions in the literature.[3,4]) Like common emulsions, nanoemulsions allow transport or solubilization of hydrophobic substances within a water-based phase. Nanoemulsions can thus be envisioned as carriers in cosmetic and pharmacological applications. Using such systems as nanocarriers for biomedical applications, through parenteral administration, has for example been shown to be efficient in solubilizing, protecting, and targeting contrast agents or drugs to specified organs, tissues, or cells for imaging or treatment purposes.[5−9] Such an approach can be expected to improve current cancer diagnostics and therapies.[7,10] Small droplet size and PEG coverage are critical for that purpose as they allow significantly improved drug biodistribution, principally by avoiding recognition by the immune system.[9]

By contrast with microemulsions, nanoemulsions generally require energy input to be produced. Indeed, whereas microemulsions are thermodynamically stable states, nanoemulsions are normally considered to be metastable systems. Indeed, the energy given to the system is used to overcome the surface free energy required to increase interfacial area between the two phases and finely disperse one phase into the other. Different methods have been introduced at laboratory and industrial scales: mechanical stirring, high-pressure homogenization, or ultrasonics.[11] Using ultrasound to produce emulsions has attracted increasing attention thanks to lower energy consumption, the decrease of surfactants use, and the achievement of smaller droplet sizes while obtaining more homogeneous batches than with conventional mechanical processes.[12]

In terms of their stability, microsized and nanosized emulsions often show remarkable behavior. Once formed, they may be stabilized for a few hours to years depending on formulation and process parameters.[13−16] Among the most important features to consider are the mutual solubilities of the two phases and the amount and types of surfactants used.[13,14] Indeed, several different destabilization phenomena may occur. Some of them involve droplet adhesion and are generally reversible; others, related to particle size evolution, are irreversible.[12] Reversible flocculation

*Corresponding authors: Tel +33 438 780 325, Fax +33 438 785 787, e-mail anne-claude.couffin@cea.fr (A.-C.C.); Tel +33 438 784 670, Fax +33 438 785 787, e-mail isabelle.texier-nogues@cea.fr (I.T.); Tel +33 140 795 219, e-mail jerome.bibette@espci.fr (J.B.).

(1) Tadros, T.; Izquierdo, P.; Esquena, J.; Solans, C. *Adv. Colloid Interface Sci.* **2004**, *108−109*, 303–318.
(2) Mason, T. G.; Wilking, J. N.; Meleson, K.; Chang, C. B.; Graves, S. M. *J. Phys.: Condens. Matter* **2007**, *19*, 079001.
(3) El-Aasser, M. S.; Sudol, E. D. *J. Coat. Technol. Res.* **2004**, *1*, 21–31.
(4) Solans, C.; Izquierdo, P.; Nolla, J.; Azemar, N.; Garcia-Celma, M. J. *Curr. Opin. Colloid Interface Sci.* **2005**, *10*, 102–105.
(5) Goutayer, M.; Dufort, S.; Josserand, V.; Royère, A.; Heinrich, E.; Vinet, F.; Bibette, J.; Coll, J.; Texier, I. *Eur. J. Pharm. Biopharm.* **2010**, *75*, 137–147.
(6) Texier, I.; Goutayer, M.; Da Silva, A.; Guyon, L.; Djaker, N.; Josserand, V.; Neumann, E.; Bibette, J.; Vinet, F. *J. Biomed. Opt.* **2009**, *14*, 054005.
(7) Andrieux, K.; Desmaële, D.; D'Angélo, J.; Couvreur, P. *Actual. Chim.* **2003**, No.Nov-Dec, 135–139.
(8) Torchilin, V. P. *Adv. Drug Delivery Rev.* **2006**, *58*, 1532–1555.
(9) Torchilin, V. P. In *Nanoparticulates as Drug Carriers*, Torchilin, V. P., Ed.; Imperial College Press: London, 2006; pp 1−8.
(10) Hervella, P.; Lozano, V.; Garcia-Fuentes, M.; Alonso, M. J. *J. Biomed. Nanotechnol.* **2008**, *4*, 276–292.
(11) Jafari, S. M.; Assadpoor, E.; He, Y.; Bhandari, B. *Food Hydrocolloids* **2008**, *22*, 1191–1202.
(12) Abismail, B.; Canselier, J. P.; Wilhelm, A. M.; Delmas, H.; Gourdon, C. *Ultrason. Chem.* **1999**, *6*, 75–83.
(13) Bibette, J.; Calderon, F. L.; Poulin, P. *Rep. Prog. Phys.* **1999**, *62*, 969–1033.
(14) Capek, I. *Adv. Colloid Interface Sci.* **2004**, *107*, 125–155.
(15) El-Jaby, U.; Cunningham, M.; McKenna, T. E. *Ind. Eng. Chem. Res.* **2009**, *48*, 10147–10151.
(16) Henry, J. V. L.; Fryer, P. J.; Frith, W. J.; Norton, I. T. *J. Colloid Interface Sci.* **2009**, *338*, 201–206.

may lead the system to cream or sediment. Meanwhile, irreversible droplet size increase may occur through two different mechanisms: Ostwald ripening and coalescence.

Coalescence occurs when two droplets collide and finally merge. When coalescence is the main destabilization mechanism, the time evolution of the average droplet size can follow very different behaviors: from perfectly homogeneous growth (monomodal distribution whose average size increases in time) to strongly heterogeneous growth (plurimodal distribution with the possibility of very early phase separation). Except in particular cases, the heterogeneous case is the rule.[14,17,18] Whereas this is generally the dominant mechanism of destabilization for micrometer-sized emulsions, coalescence is classically prevented with nanoemulsions. The small droplet size prevents nanoemulsions from undergoing reversible aggregation mechanisms that, when coupled to gravity, may accelerate coalescence because of the net increase in contact film duration. Indeed, droplet adhesion decays with droplet diameter,[19] which allows nanoemulsions to be protected against flocculation phenomena. Therefore, the main nanoemulsion destabilizing route to be overcome concerns the Ostwald ripening process.

Ostwald ripening is defined as the growing of the largest droplets at the expense of the smallest ones. This occurs because of the chemical potential difference of the oil between droplets of different sizes, due to different curvature radii. Indeed, as this chemical potential increases when decreasing droplet size, due to the Laplace pressure increase, the smallest droplets tend to give material to the largest ones through mass transfer across the continuous phase. The droplet size evolution as a function of time can be described by the LSW theory (Lifshitz−Slyozov−Wagner).[20,21] The Laplace pressure of nanoemulsions can exceed several atmospheres,[1,14] explaining thus the predominant role of this phenomenon in destabilizing small droplets.

Herein, the parameters governing the long-term stability of nanoemulsions are carefully addressed, as is the fragmentation route obtained using ultrasonics. Finally, we comment about the relationship, or lack of one, between equilibrium microemulsions and the nanoemulsions studied here.

Materials and Methods

1. Materials. Suppocire NC and Labrafac are kindly donated by Gattefossé (Saint-Priest, France). The PEG stearates Myrj s40, Myrj s50, Myrj s100 (poly(ethylene glycol) 40 stearate, 50 or 100 stearate), and Super-refined Soybean oil are gifts from CRODA (Chocques, France). Lipoid s75 is purchased from Lipoid GmbH (Ludwigshafen, Germany), and other chemical products are from Sigma-Aldrich (Saint Quentin Fallavier, France).

2. Nanoemulsion Fabrication. Nanoemulsion droplets are composed of a lipid core comprising a mixture of oil (Super-refined soybean oil or Labrafac) and wax (Suppocire NC), stabilized by a surfactant shell comprising a mixture of phospholipids (lipoid s75) and PEG-surfactants (Myrj s40, Myrj s50, or Myrj s100), and dispersed in an aqueous phase (NaCl 154 mM or PBS 1X (NaCl 154 mM/0.1 M Na_2HPO_4/pH 7.4)). The studied compositions do not lead to an equilibrium microemulsion: no micelle swelling is observed over time, and no microemulsion phase is obtained, even after prolonged oil exposure (more than 4 days). Nanoemulsions are then prepared by ultrasonication. The aqueous phase and the lipid phase are first prepared. The lipid phase results from a mixture of solid and liquid glycerides and the insoluble surfactant Lipoid s75, while the aqueous phase is composed of the hydrophilic surfactant Myrj s40, Myrj s50, or Myrj s100 in aqueous buffer. After homogenization at 45 °C, the two phases are crudely mixed and sonication cycles are performed at 45 °C during a 20 min period, amounting to 5 min of actual sonication (alternation 10 s sonication/30 s without sonication). A conical tip sonicator instrument (AV505 Ultrasonic processor, Sonics) with a 3 mm diameter probe is used. Different sonication powers (P_s) have been employed. The acoustic power is directly controlled by the instrument. Qualitative values of sonication power are given as percentage of the maximum power of the machine. Quantitative values of energy are given when plotting as a function of the total energy input (J). The volume of all the samples is 2 mL, sonicated in similar 5 mL vials.

For convenience, mixtures of solid and liquid lipids are noted NCXX in the text and figures below, where XX defines the weight fraction of wax: $XX = w_{wax}/(w_{wax} + w_{oil})$.

3. Microemulsion Investigation. The ternary system tetradecane/C12EO5/water, known to form microemulsion phases,[22−24] is used to evaluate nanoemulsion behavior when a monophasic microemulsion also exists. The study is carried out at 35 °C and the surfactant concentration fixed at 16.6% w/w. Experiments with and without ultrasonication are compared for compositions in the monophasic microemulsion domain (12% oil w/w) and in the biphasic domain comprising microemulsion + phase-separated oil (16% oil w/w). The sample volume is 2 mL throughout.

4. Size Distribution Monitoring during Sonication and Stability Studies. Droplet size distributions are characterized by dynamic light scattering (DLS) on a NanoZS machine (Malvern, France). Measurements are done at a fixed angle of 173° using a 633 nm laser with each data point being the average of three independent measurements performed on an automatic mode (> 20 runs of 10 s each). All samples are measured in aqueous buffer at a dispersed phase weight fraction of 0.1% to avoid multiple scattering effects. Before measurement at 25 °C, samples are left to equilibrate for 2 min. Average diameter and polydispersity are extracted from cumulant analysis of the autocorrelation function on an intensity basis. DLS data are measured on an intensity basis; number distribution can then be derived, assuming the Mie theory is fulfilled, and inputting the complex refractive index of the material. LSW theory for Ostwald ripening requires the number-average radius r_N, but as reported by Kabalnov et al., for particles smaller than 100 nm, $r_I = 1.18 r_N$ (r_I and r_N respectively being the average radius of the intensity and number distributions).[25] Consequently, working on an intensity basis should not affect reasoning but simply add a prefactor to the measured droplet size. Nanoemulsion stability is thus assessed by measuring the droplet size as a function of the storage time through this method. Each experimental point is the average and standard deviation of measurements on three independently fabricated samples. Similarly, for the emulsification study, nanoemulsion size distributions are monitored during sonication by taking samples at specified time intervals (t_0 + 1, 2, 5, 8, 10, 15, 20 min and sometimes 25 and 30 min) and characterizing them by DLS. In parallel, nanoemulsion appearance is monitored during sonication by taking photographs at similar time intervals. The time evolution of nanoemulsion droplet size is fitted by a first-order exponential decay with Origin software.

Results

1. Nanoemulsion Production by Ultrasonication. *a. Size Distribution Monitoring during Emulsification.* The

(17) Deminiere, B.; Colin, A.; Leal-Calderon, F.; Muzy, J. F.; Bibette, J. *Phys. Rev. Lett.* **1999**, *82*, 229–232.
(18) Deminiere, B.; Stora, T.; Colin, A.; Leal-Calderon, F.; Bibette, J. *Langmuir* **1999**, *15*, 2246–2249.
(19) Poulin, P.; Bibette, J. *Phys. Rev. Lett.* **1997**, *79*, 3290–3292.
(20) Lifshitz, M.; Slyozov, V. V. *J. Phys. Chem. Solids* **1961**, *19*, 35–50.
(21) Wagner, C. *Z. Elecktrochem.* **1961**, *65*, 581–594.
(22) Olsson, U.; Shinoda, K.; Lindman, B. *J. Phys. Chem.* **1986**, *90*, 4083–4086.
(23) Lichterfeld, F.; Schmeling, T.; Strey, R. *J. Phys. Chem.* **1986**, *90*, 5762–5766.
(24) Cabane, B.; Henon, S. In *Liquides: Solutions, Dispersions, Émulsions, Gels*; Belin: Paris, 2003; pp 271−276.
(25) Kabalnov, A. S. *Colloid J. USSR* **1991**, *53*, 709–713.

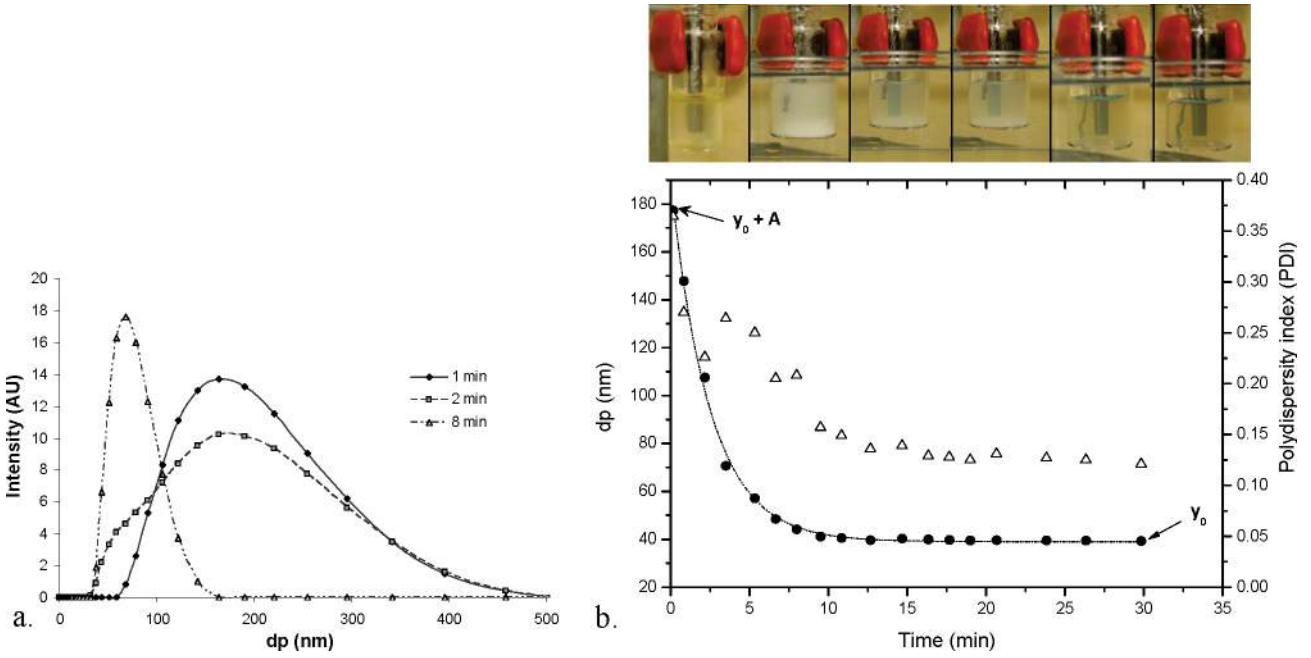

Figure 1. Complete monitoring during emulsification by ultrasonication: (a) evolution of droplet size distribution; (b) dispersion appearance (photographs), particle mean diameter (black disks), and polydispersity index (open triangles) (power of sonication: 25%).

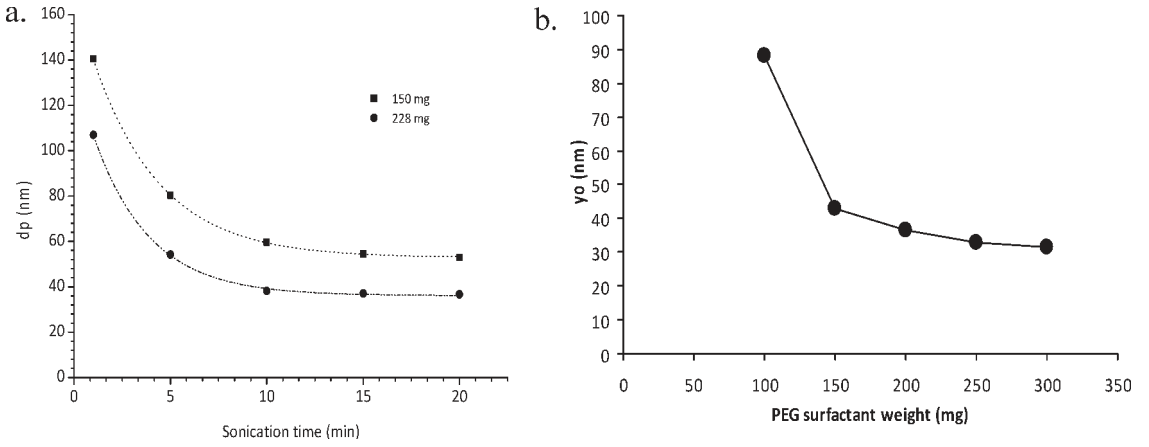

Figure 2. Effect of the amount of hydrophilic surfactant used on (a) emulsification kinetics and (b) the saturated size y_0. (a) Formulations used: 200 mg of NC75; 100 mg of Lipoid s75; X mg of Myrj s50; 1.45 mL of PBS. (b) Formulations used: 200 mg of NC75; 100 mg of Lipoid s75; X mg of Myrj s40; 1.45 mL of PBS (X defines the experimental variable; power of sonication: $P_s = 25\%$).

nanoemulsion system studied here is composed of a lipid core (oil and wax), stabilized by a mixture of insoluble surfactants (phospholipids) and hydrophilic surfactants (PEG stearate), which polyoxyethylene chain length can be varied. The evolution of size distribution along sonication can be seen in Figure 1a: starting from a very broad monomodal distribution, the final monodisperse distribution is obtained after crossing a bimodal distribution region at times 2−5 min, which corresponds to a dramatic polydispersity increase (Figure 1b). In order to follow the emulsification process during ultrasonication, the mean droplet diameter (d_p), polydispersity index, and suspension appearance are recorded at specified time intervals (Figure 1b). The size evolution can be fitted with a monoexponential function of sonication time, with parameters y_0 describing the saturation diameter of droplets and τ the characteristic decay time:

$$d_p(t) = y_0 + A\mathrm{e}^{(t-t_0)/\tau} \quad (1)$$

Here d_p is the mean droplet diameter, whereas A and $t_0 = 1$ min are used to fit to the first measurable value of the mean droplet size $y_0 + A$. Before the time t_0 (which corresponds to two sonication episodes), no average size or polydispersity index can be recorded as the system is extremely heterogeneous, being a crude mixture of both immiscible phases. This monoexponential fit gives very good regression coefficients (>0.99), while power law fitting, classically employed for polymer or carbon nanotube scission under sonication, is much less accurate (data not shown).[26,27] With this simple procedure, the influence of both composition and process parameters (P_s: power of sonication; t_s: time of sonication) on the final saturated size y_0 and the characteristic decay time, τ, are investigated. Numerical values of the fitting parameters are given in the Supporting Information.

(26) Lucas, A.; Zakri, C.; Maugey, M.; PAsquali, M.; Van der Schoot, P.; Poulin, P. *J. Phys. Chem. C* **2009**, *113*, 20599–20605.
(27) Hennrich, F.; Krupke, R.; Arnold, K.; Rojas Stütz, J. A. R.; Lebedkin, S.; Koch, T.; Schimmel, T.; Kappes, M. M. *J. Phys. Chem. B* **2007**, *111*, 1932–1937.

b. Parameters Affecting the Saturated Size y_0. The influence on the saturated size y_0 of the surfactant type and concentration of both insoluble and hydrophilic surfactants is investigated. The amount of hydrophilic surfactant (Figure 2) and the length of the PEG chain of this surfactant (Figure 3) are systematically varied at fixed amount of oil, added wax, and water phase. When increasing the amount of PEG surfactant, y_0 dramatically decreases until reaching a plateau: for instance, for a polyoxyethylene 40 stearate (Myrj s40) a weight of about 200 mg/2 mL sample is needed to reach a size between 30 and 40 nm diameter (Figure 2). A similar trend is observed with the insoluble surfactant (data not shown). In parallel, as shown in Figure 3, changing the length of the PEG chain of the hydrophilic surfactants leads to different droplet sizes, presumably connected with changes in the surface tension and/or PEG chain conformation.[28] The longer the PEG chains, the larger the droplet sizes. This may be linked to the observed reduction in surface tension from 4.71 ± 0.36 mN m^{-1} for PEG_{100} (Myrj s100) down to 3.10 ± 0.15 mN m^{-1} for PEG_{20} (Myrj s20) (macroscopic values obtained by pending drop measurements). Conversely, as discussed further below, neither the dispersed phase weight fraction (Figure 4a), nor the continuous phase viscosity (Figure 4b), nor even the sonication power (Figure 5) affects the saturated size y_0.

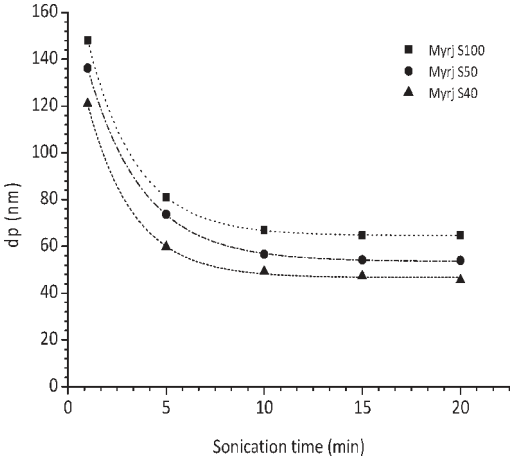

Figure 3. Effect of the PEG chain length of the hydrophilic surfactant. Formulations used: (a) 200 mg of NC75; 100 mg of Lipoid s75; 0.1 mM Myrj sX; 1.45 mL of PBS (X defines the experimental variable; power of sonication: $P_s = 25\%$).

c. Parameters Affecting Emulsification Kinetics. Different parameters can affect the emulsification kinetics and the associated characteristic decay time τ. Neither the hydrophilic surfactant characteristics (length of the PEG chain and amount) nor the viscosity of the samples significantly influences τ. Indeed, τ is only slightly decreased upon increase of the surfactant concentration (Figure 2a), while it is not significantly affected by the length of the PEG chain of the hydrophilic surfactant (Figure 3). Similarly, τ is only slightly lowered upon dilution of the sample (Figure 4a) or upon increase of the continuous phase viscosity, through the addition of glycerol as viscosity enhancer (Figure 4b). All these parameters have in fact a small influence on the emulsification kinetics. By contrast, increasing sonication power significantly reduces τ until it reaches a plateau for large sonication powers ($P_s > 30\%$) (Figure 5).

If sonication is performed over sufficient time, the saturated size y_0 is reached whatever the sonication power. However, for lower power the time to reach saturation is much increased. This may indicate that at constant composition the energy provided to the system is the major control parameter. Indeed, as shown in Figure 6, all curves of Figure 5a fall on top of each other when plotted as a function of the total energy input (power of sonication × time of sonication). This strongly suggests that emulsification efficiency only depends on the overall total energy density put into the system (note that as a constant sample volume is used in this study, energy and energy density are equivalent).[29]

2. Nanoemulsion Stability. *a. Simple Ostwald Ripening.* Emulsions composed of a pure oil core (Labrafac, triglycerides C8−C10) and a PEG surfactant outer layer (Myrj s40) are first used as an extremely simplified model. This simple system exhibits a significant size increase over time, as evidenced by the cube of droplet radius versus time (Figure 7a). Ostwald ripening rates ω can be predicted by the LSW theory (eq 2),[20,21] where r is the average droplet radius, γ is the interfacial tension, V_m and ρ are the oil molar volume and density, D and C_∞ are respectively the diffusion coefficient and the solubility of the dispersed phase in the continuous phase and finally, R is the gas constant, and T is the absolute temperature:

$$\omega = \frac{dr^3}{dt} = \frac{8}{9}\frac{C_\infty \gamma V_m D}{\rho RT} \quad (2)$$

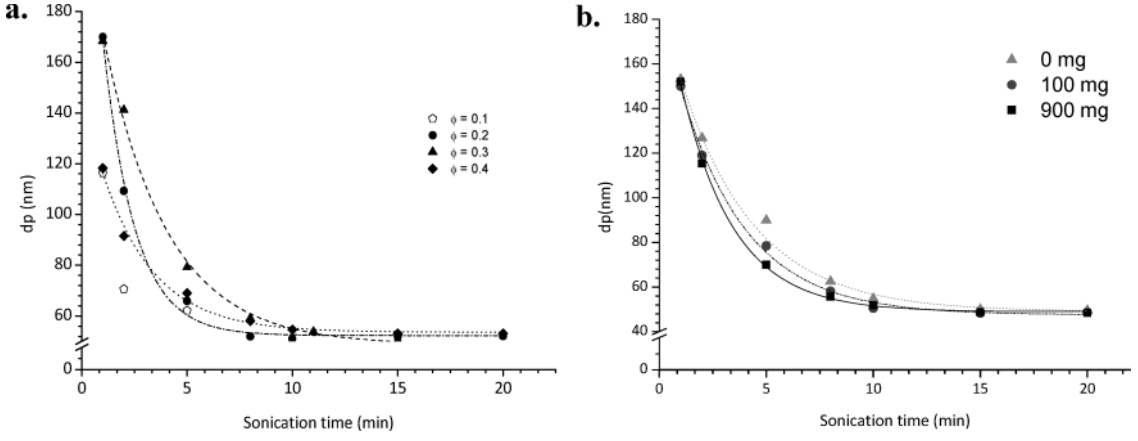

Figure 4. Effect of sample viscosity on emulsification: size monitoring for (a) different weight fractions of the dispersed phase and (b) different continuous phase viscosities. (a) Formulations used: constant dispersed phase composition: 45.3% NC75; 46% Myrj s40; 8.7% Lipoid s75 with varying dispersed phase weight fraction $\Phi = X$ ($V = 2$ mL). (b) Formulations used: 340 mg of NC75; 65 mg of Lipoid s75; 345 mg of Myrj s40; 2.25 mL of PBS; X mg of glycerol (X defines the experimental variable; $P_s = 25\%$).

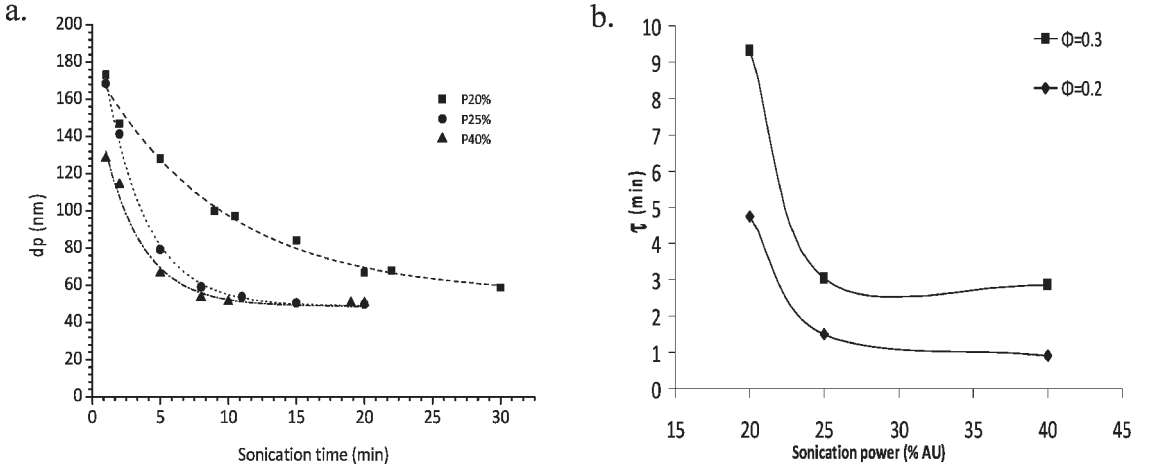

Figure 5. Effect of process parameters on emulsification: (a) size monitoring for different sonication powers; (b) evolution of the characteristic decay time as a function of the sonication power and dispersed phase weight fraction Φ. Formulations used: (a) 272 mg of NC75; 276 mg of Myrj s40; 52 mg of Lipoid s75; 1400 mg of NaCl 154 mM (dispersed phase weight fraction: $\Phi = 0.3$). (b) Reported results of Figures 3 and 4a.

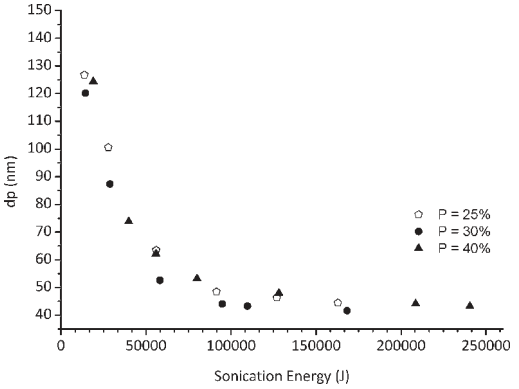

Figure 6. Size monitoring curves as a function of the total energy input. Formulations used: 272 mg of NC75; 276 mg of Myrj s40; 52 mg of Lipoid s75; 1400 mg of NaCl 154 mM (dispersed phase weight fraction: $\Phi = 0.3$).

For different storage temperatures, ranging from room temperature to 70 °C, Ostwald ripening plots exhibit a linear relationship between the cube of the droplet radius and time, indicating that Ostwald ripening is the major destabilization mechanism (Figure 7a).

Moreover, Ostwald ripening rates are temperature-dependent, displaying an exponential relationship with the inverse of storage temperature (Figure 7b). Ostwald ripening rates thus follow an Arrhenius law that can be accounted for by similar laws ruling both the solubility and the diffusion coefficient of the dispersed phase in the continuous phase (eqs 3 and 4).

$$C_\infty = C_{0\infty} \exp(-W/RT) \tag{3}$$

$$D = \frac{k_B T}{6\Pi\eta r} \quad \text{with } \eta = \eta_0 \exp(-E_a/k_B T) \tag{4}$$

On the other hand, the parameters V_m, γ, and ρ of eq 2 are not significantly affected by temperature. As explained in eq 5, it therefore leads the Ostwald ripening rate to follow the Arrhenius law (eq 6).

$$\omega = \frac{8}{9}\frac{\gamma V_m}{\rho RT}[C_{0\infty} \exp(-W/RT)]\left[\frac{k_B T}{6\Pi r \eta_0 \exp(-E_a/k_B T)}\right] \tag{5}$$

$$\omega \propto \omega_0 \exp\left(-\frac{W' + E_a'}{T}\right) \tag{6}$$

While serving as a useful benchmark for the Ostwald ripening process, this first nanoemulsion composition is quite unstable, with a droplet size that rapidly increases until finally reaching phase separation, giving two macroscopic separated domains of oil and water.

b. Stabilization by Combination of Trapped Species Both at the Membrane and within the Core. The role of the droplet surfactant monolayer (membrane) composition is first investigated by formulating nanoemulsions of pure Labrafac at similar droplet diameters (≈50 nm) with different weight ratios of insoluble surfactant (lecithin) to hydrophilic surfactant (PEG surfactant) (Table 1). These two surfactants have very different solubilities in the aqueous phase, with lecithin being almost insoluble. As possible destabilization mechanisms could occur through the interface, the stability study is conducted with all samples diluted to a constant total nanoparticle surface of 2×10^{13} nm^2 for 1 mL of colloidal dispersion, at the start of experiments. Two different time scales have to be considered. At short time ($t < 20$ h), Ostwald plots are linear, presenting very good regression coefficients (> 0.9) as displayed in Figure 8. At longer times, linearity is degraded which probably reveals that coalescence might be acting, too. As far as Ostwald ripening is concerned (short times), adding the insoluble surfactant significantly lowers the rate of droplet growth (Figure 8a). It is well-known that the Ostwald process can be eliminated or reduced by encapsulating insoluble species in the core[30−32] because shrinkage of small droplets is opposed by a buildup of osmotic pressure

(28) Allen, C.; Dos Santos, N.; Gallagher, R.; Chiu, G. N. C.; Shu, Y.; Li, W. M.; Johnstone, S. A.; Janoff, A. S.; Mayer, L. D.; Webb, M. S.; Bally, M. B. *Biosci. Rep.* **2002**, *22*, 225–250.
(29) Canselier, J. P.; Delmas, H.; Wilhelm, A. M.; Abismail, B. *J. Dispersion Sci. Technol.* **2002**, *23*, 333–349.
(30) Wooster, T. J.; Golding, M.; Sanguansri, P. *Langmuir* **2008**, *24*, 12758–12765.
(31) Egger, H.; McGrath, K. M. *J. Colloid Interface Sci.* **2006**, *299*, 890–899.
(32) Webster, A. J.; Cates, M. E. *Langmuir* **1998**, *14*, 2068–2079.

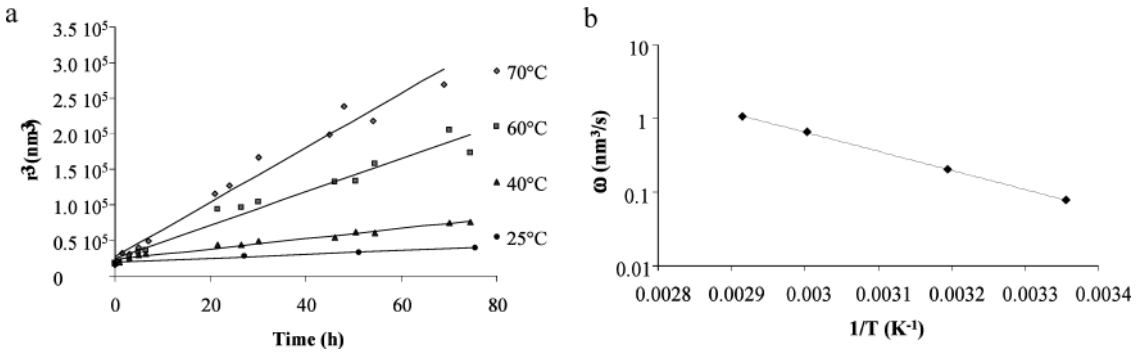

Figure 7. Simple Ostwald ripening as a function of storage temperature: (a) size evolution; (b) Ostwald ripening rates. Sample sizes are monitored for different storage temperatures (25, 40, 60, and 70 °C), and Ostwald ripening rates are extracted over 90 h experiments. Formulations used: 440 mg of Labrafac; 200 mg of Myrj s40; 1200 mg of NaCl 154 mM.

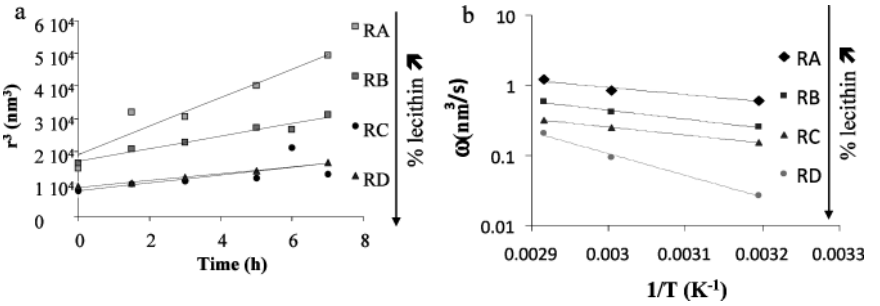

Figure 8. Effect of trapped species at the membrane on Ostwald Ripening at short time (t < 8 h): (a) size evolution at 70 °C; (b) Arrhenius plots. Droplet sizes are monitored for different storage temperatures (25, 40, 60, and 70 °C), and Ostwald ripening rates are extracted over 8 h experiments.

Table 1. Nanoemulsion Compositions Used for the Membrane Composition Study (Weights in mg)

				dispersed phase		
			continuous phase	membrane		core
composition	droplet initial average diameter (nm)	Lipoid s75/Myrj s40 weight ratio	saline solution (NaCl 154 mM)	Myrj s40	Lipoid s75	Labrafac
RA	52 ± 2	0	1200	200	0	440
RB	56 ± 2	0.188	1250	345	65	340
RC	53 ± 2	0.45	1300	200	90	210
RD	53 ± 2	1	1300	150	150	150

(increasing free energy) of the trapped component. As evidenced here, this concept of trapped species can equally be extended to the surfactant membrane, where the presence of an insoluble component similarly prevents the disappearance of small droplets. As previously described, Ostwald ripening rates follow an Arrhenius law of the inverse of temperature (Figure 8b). Interestingly, the activation energy E_a, given by the slope of the plot, is not significantly affected by the lecithin content, but the intercept of the plots ω_0 significantly decreases when increasing lecithin. It additionally highlights the role of lecithin in stabilizing the droplets, giving smaller Ostwald ripening rates.

It is possible to identify a range of membrane composition promoting good long-term stability (t > 90 h): 0.15 < ratio lecithin/PEG surfactant < 0.6 (w/w) (Figure 9). Too low lecithin content leads to droplet destabilization by Ostwald ripening, whereas too low PEG surfactant concentration leads probably to increase in droplet coalescence. Indeed, PEG surfactants are known to provide droplets with an efficient steric repulsion against coalescence, while PEG-deprived droplets are only protected by the modest electrostatic repulsion provided by the lecithin heads. The stability limit achieved by trading off these two behaviors is observed in the range of 20−40 h after nanoemulsion preparation, depending on the storage temperature used.

To study the more conventional suppression of Ostwald ripening by trapped species in the core of the droplets, nanoemulsions are then prepared using a formulation in which the core is composed of complex mono-, di-, and triglycerides mixture (different weight ratios of oil and wax), keeping the same composition of hydrophilic and insoluble surfactants at the interface (ratio lecithin/PEG surfactant = 0.188). Although the wax involved is solid at room temperature, the nanoemulsion droplet core remains liquid at temperature above 20 °C (observed by DSC and NMR analysis, data not shown). When adding as little as 10% w/w of wax in core composition, the growth is almost stopped (Figure 10). This feature is observed for all storage temperatures but is even more spectacular for elevated temperature (70 °C) as shown in Figure 11b. Linear Arrhenius plots are again obtained as long as Ostwald ripening rates are not negligible (wax content ≤10% w/w) (Figure 11b). Here again, ω_0, the intercept of the plot with the y axis, dramatically decreases while increasing wax content, highlighting again its stabilizing effect. Nonetheless, this time, the activation energy E_a is significantly

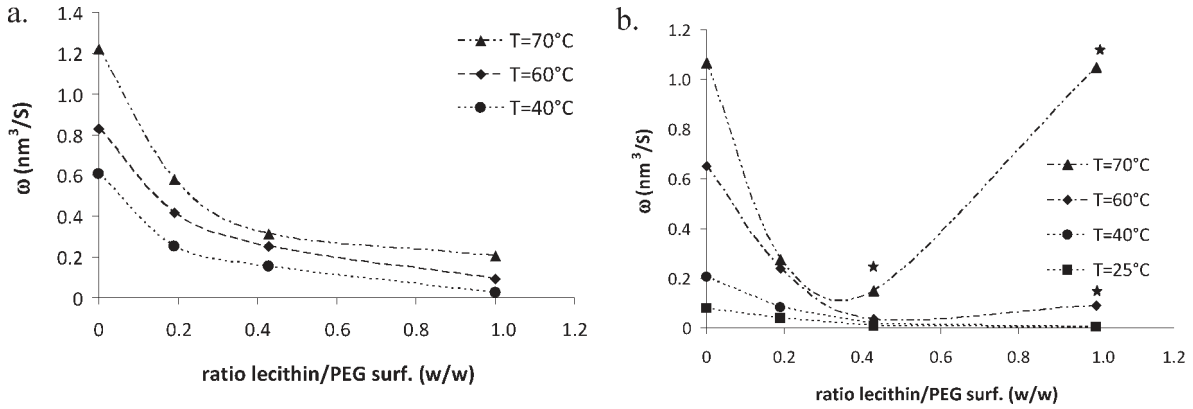

Figure 9. Effect of trapped species at the membrane on Ostwald ripening at (a) short time ($t < 8$ h) and (b) long time ($t < 90$ h). Sample sizes are monitored for different storage temperatures (25, 40, 60, and 70 °C), and Ostwald ripening rates are extracted over 8 h experiments for (a) and 90 h for (b). ★: "fictitious" Ostwald ripening rates are extracted even though Ostwald ripening plots present degraded linearity. This indicates that Ostwald ripening is not the only mechanism at the origin of destabilization; coalescence needs also to be considered, which is beyond the scope of these fits.

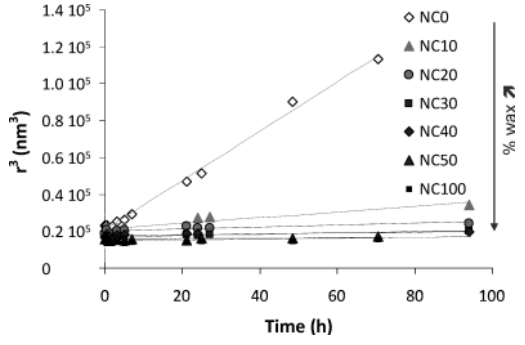

Figure 10. Effect of encapsulated species in the core on Ostwald ripening size evolution at 70 °C. Sample sizes are monitored over 90 h at 70 °C. Formulations used: 345 mg of oil/wax mixture (Labrafac/Suppocire); 340 mg of Myrj s40; 65 mg of Lipoid s75; 1250 mg of NaCl 154 mM.

lowered, converging to zero, upon addition of wax in the core. These findings are consistent with previously reported data[30−33] in which addition of insoluble species such as long chain triglycerides in the nanoemulsions has been tested. No temperature study has nevertheless been previously reported to the extent of our knowledge.

Discussion

1. Nanoemulsion Production by Ultrasonication. To produce nanoemulsions, sufficient energy needs to be provided to the system in order to create the required interface area. Droplet breakup occurs when the applied shear is greater than the Laplace pressure of the droplets. For the dilute case (at low oil volume fractions), Taylor[34] predicts that the emulsion diameter d_p must scale as

$$d_p \propto \frac{2\gamma}{3\eta\dot{\varepsilon}} \quad (7)$$

where γ is the interfacial tension, η the continuous phase viscosity, and $\dot{\varepsilon}$ the shear rate. Aiming for 20 nm oil droplets, shear rates up to 10^9 s^{-1} are necessary.[2,34,35] Only a few methods can achieve such shear rates, and the most commonly employed are high-frequency ultrasonic devices or microfluidizers. The final droplet diameter in principle results from two opposite processes: droplet breakup and coalescence.[1,2,36] However, two different regimes can be isolated depending on the influence/importance of coalescence: a "surfactant-poor regime" in which coalescence is occurring during sonication and a "surfactant-rich regime" for which such coalescence can be neglected.[37] It is known that emulsification by ultrasonication relies on the nucleation, growth, and collapse of gas bubbles in the medium, creating a strong hydrodynamic flow field in the surrounding liquid.[26,38−42] This phenomenon is known as cavitation. Strain rates of up to 10^9 s^{-1} are theoretically predicted for the radial elongational flow near a cavitation bubble.[26] This high strain rate can explain the efficiency of sonication at creating very small emulsion droplets.

In the present study, it is observed that, once a pre-emulsion is formed, the time evolution of droplet diameter can be described using first-order kinetics with an exponential decay. By contrast, as indicated above, the scission kinetics of polymer chains or carbon nanotubes have been described using scaling power laws.[26] These laws are related to the successive scissions of chains or nanotubes as a function of time. The observation of an exponential decay suggests that very small droplets could be obtained with a final size y_0 in a single step during the sonication process. One big droplet would be shattered into several small droplets. The difference from other materials may originate from the liquid state and deformability of emulsion drops, the high surfactant concentration promoting the stabilization of the newly created interfaces. The exponential decay also supports the idea that the formed small droplets do not significantly coalesce (which would lead to slight deviation to the first-order exponential kinetics) as in the "surfactant-rich regime" defined by Taisne et al.[37] When the ultimate saturated size is reached, approximately 10−15% w/w of the total surfactants would remain in the continuous phase (value obtained by assuming a theoretical 2 surfactant molecules/nm^2 at the interface), in agreement with the

(33) Jiao, J.; Burgess, D. J. *J. Colloid Interface Sci.* **2003**, *264*, 509–516.
(34) Taylor, G. I. *Proc. R. Soc. London, Ser. A* **1934**, *A146*, 501.
(35) Leong, T. S. H.; Wooster, T. J.; Kentish, S. E.; Ashokkumar, M. *Ultrason. Sonochem.* **2009**, *16*, 721–727.
(36) Walstra, P. *Chem. Eng. Sci.* **1993**, *48*, 333–349.
(37) Taisne, L.; Walstra, P.; Cabane, B. *J. Colloid Interface Sci.* **1996**, *184*, 378–390.
(38) Crum, L. A. *Ultrasonics* **1984**, *22*, 215–223.
(39) Kuijpers, M. W. A.; Iedema, P. D.; Kemmere, M. F.; Keurentjes, J. T. F. *Polymer* **2004**, *45*, 6461–6467.
(40) Odell, J. A.; Keller, A.; Rabin, Y. *J. Chem. Phys.* **1988**, *88*, 4022–4028.
(41) Lee, J.; Kentish, S. E.; Ashokkurnar, M. *J. Phys. Chem. B* **2005**, *109*, 5095–5099.
(42) Nguyen, T. Q.; Liang, O. Z.; Kausch, H. H. *Polymer* **1997**, *38*, 3783–3793.

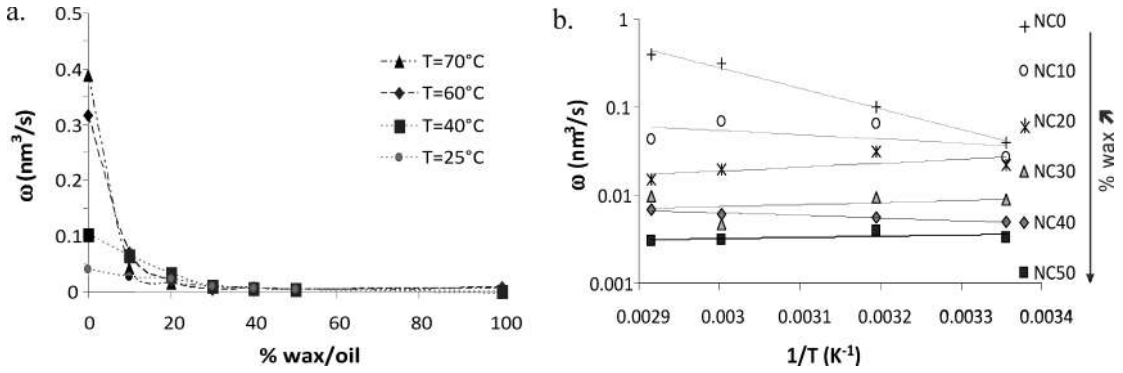

Figure 11. Effect of encapsulated species in the core on Ostwald ripening: (a) Ostwald ripening rates as a function of core composition and temperature; (b) associated Arrhenius plots. Sample sizes are monitored for different storage temperatures (25, 40, 60, and 70 °C), and Ostwald ripening rates are extracted over 90 h experiments.

postulated surfactant-rich regime. Therefore, each globule evolves individually, undergoing scissions which ultimately lead to the obtainment of droplets at the saturated size y_0. More precisely, because polydispersity rises up when the average size suddenly drops (Figure 1b), droplets may directly reach the final saturated size when encountering the ultrasonic stress, on a one-step basis. The dramatic polydispersity increase may thus be explained by the large difference between the droplets that have undergone a cavitational stress (and reached the final saturated size) and the ones that have not yet (and present a 150−200 nm rough average diameter), as suggested by the size distribution represented in Figure 1a. The mean droplet diameter levels off at long times until full surfactant consumption and fragmentation of all the big drops. The formed small droplets exhibit a large Laplace pressure and can sustain the hydrodynamic stress of collapsing bubbles without being fragmented into smaller ones.

As shown previously, the decrease of the mean droplet size is described by a characteristic decay time that mainly depends on sonication power. Modulating the sonication power P_s is expected to change the instantaneous concentration of collapsing bubbles, through the further propagation of acoustic waves and probability of nucleating cavitation bubbles. Thus, it increases the probability for a given droplet to undergo a cavitational stress, provided the acoustic pressure, directly linked to the sonication intensity, is greater than the pressure of Blake to initiate the cavitation phenomenon (which appears to always be the case over the whole investigated range of sonication powers).[29,39] Therefore, increasing the sonication power leads more droplets to undergo scission over the same time t_s of sonication, shortening the time needed to reach the saturated size. The observed saturation effect on τ, when increasing the sonication power above a certain threshold (Figure 5b), can be understood when considering that the concentration of cavitating bubbles has an upper limit. Indeed, cavitation occurs in a small volume around the sonotrode. This volume increases until it reaches the overall container. This limiting bubble density is thus given by the maximum number of bubbles that can be formed in the container volume. The mean droplet diameter evolution as a function of time, or the evolution of the mean droplet diameter as a function of the overall energy input $E = P_s t_s$, should follow the same scaling, since E and t are linearly related (Figure 6). In addition, when expressed as a function of E, all plots merge together. This can merely be understood by considering that the overall energy density given to the system, E_v, is directly linked to the overall number of effective collapsing events.

In contrast to the prediction of the simple Taylor model (eq 7), we observe no influence of continuous phase viscosity, or dispersed phase weight fraction, on the final saturated size (Figure 4). This has already been reported for a wide range of continuous phases, but also dispersed phase viscosities.[43] The simple Taylor model is only valid for highly diluted suspensions, which is not the case of this study. However, as shown previously, this model can still be used to estimate the order of magnitude of droplet ultimate size that can be achieved using ultrasonication characteristic shear rate. Folger considers that shock waves, produced by cavitation events, are responsible for droplet size decrease.[44] The leading parameters are thus the ones affecting cavitation: surely, the hydrostatic pressure and the gas content of the liquid, but not the liquid viscosity which has no influence during this process.[29,44] We here consider that each cavitation event is powerful enough to break initial droplets to their final saturated size. The average size distribution time evolution, followed by DLS (Figure 1b), mainly reflects the evolution of the number of large droplets. Considering the probability p for a droplet to undergo a cavitation event to be constant with time, the number of large size droplets would decay exponentially with time, leading d_p to follow similar scaling law. Viscosities of the continuous and dispersed phases have consequently no influence on p and therefore the size decrease kinetics (Figure 4b). On the contrary, increasing the fraction of dispersed phase for a given sonication power significantly enhances the probability p of a cavitational event to occur in the vicinity of dispersed phase droplet (Figure 4a). Similarly, increasing the concentration of collapsing events, by applying a more intense sonication power, leads to increasing the probability p for droplets to undergo cavitational stress, at fixed fraction of dispersed phase (Figure 5).

2. Nanoemulsion Stability. As previously mentioned, the very small size of nanoemulsion droplets helps to prevent them from undergoing reversible destabilization such as flocculation and creaming.[14] The small size also helps inhibiting coalescence. Indeed, the frequency of droplet coalescence essentially vanishes when the contact area becomes too small, particularly in the absence of any permanent contact.[45] Adding insoluble species in the droplet core has been shown to dramatically reduce Ostwald ripening rate thanks to entropic stabilization.[30,31,33] Adding Suppocire NC wax into the core efficiently promotes stabilization, even at low incorporation loading. This wax consists in a complex mixture of mono-, di-, and triglycerides of very different solubilities and has a sufficient insoluble component to stabilize against Ostwald ripening when present

(43) Behrend, O.; Ax, K.; Schubert, H. *Ultrason. Chem.* **2000**, *7*, 77–85.
(44) Li, M. K.; Fogler, H. S. *J. Fluid Mech.* **1978**, *88*, 499–511.
(45) Pays, K.; Giermanska-Kahn, J.; Pouligny, B.; Bibette, J.; Leal-Calderon, F. *Phys. Rev. Lett.* **2001**, *87*, 178304.

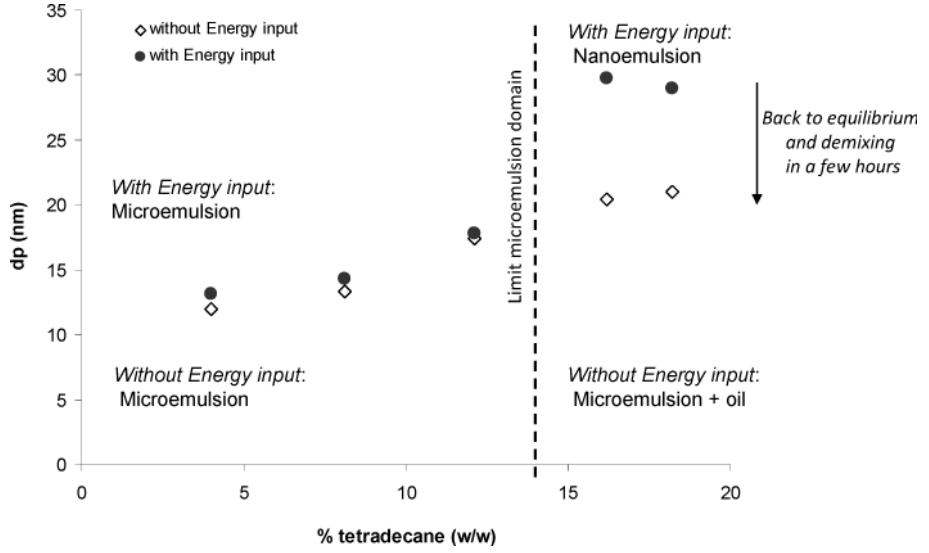

Figure 12. Microemulsion vs nanoemulsion: role of energy input.

at 10% w/w or above in the core (corresponding to a molar fraction of the insoluble component (wax) to total components (oil + wax) $X = 3\%$) (Figure 10). As already pointed out,[32] the entropic stabilization is obtained when the solute (nonsoluble species) excess osmotic pressure is roughly of the order of the Laplace pressure:

$$\frac{RTX}{v_m} \propto \frac{2\gamma}{r} \quad \text{which gives } X \propto \frac{2\gamma}{r}\frac{v_m}{RT} \tag{8}$$

Taking the molar gas constant $R = 8.314$ J K^{-1} mol^{-1}, a surface tension of $\gamma = 10^{-3}$ N m^{-1}, an oil molar volume $v_m = 1{,}000$ cm^3 mol^{-1}, and a droplet radius $r = 25$ nm, the obtained molar fraction of insoluble to soluble oil X has a value of 3.3% at $T = 298$ K. When considering the relative mass of our soluble oil and insoluble wax, this value is nicely comparable to the 10% weight fraction (3% molar fraction) experimentally observed to be sufficient to stabilize the system. In addition, we have shown that the concept of trapped species, originally developed for the core, applies to the membrane compartment as well (Figure 8), as theoretically envisioned earlier.[32,46] This opens up new formulation opportunities, allowing use of the membrane composition to provide stability, while choosing relatively soluble oil in the core if this offers the best encapsulation environment for species of interest for desired applications.

As a last discussion point, we address whether or not the behavior of the herein described nanoemulsions is significantly altered when the formulation point lies in close proximity to a domain of stable microemulsion in the pseudoternary (oil/water/surfactant) phase diagram. We therefore consider a mixture that shows spontaneous partial dissolution of bulk oil when placed in contact with an aqueous micellar solution to create a phase of swollen micelles. This does not happen in any of the formulations addressed so far, which require ultrasonication (or other mechanical energy input) to achieve any significant emulsification of the oil. We therefore chose a well-known ternary system made of tetradecane/C12EO5/water, which is able to solubilize 12% w/w of oil in the presence of 16.6% w/w surfactant.[22−24] Note that in all of the previously studied systems the surfactant percentage is quite similar. The role of ultrasonication on both the one-phase microemulsion and on the biphasic system made of the microemulsion + residual phase-separated oil (2% w/w) is then examined. No influence of ultrasonication on the microemulsion is observed, in agreement with its thermodynamically equilibrated nature (Figure 12). For biphasic samples, we observe, under ultrasonication, the almost instantaneous dissolution of oil to create swollen micelles. This is confirmed by measuring the micelle diameter right after ultrasonication treatment, which is found to be increased by 40% as reported in Figure 12. However, the system rapidly relaxes toward the initial biphasic state within a few hours. This allows us to conclude that for droplets larger than the emulsification failure limit (set by the spontaneous curvature radius of the equilibrium swollen micelles) the free energy cost of deforming the surfactant membrane is sufficient to drive rapid deswelling through the Ostwald ripening process. Accordingly, the observed stability of the nanoemulsion formulations described in previous sections is not the result of their being "almost stable" in the sense of close thermodynamic proximity to an equilibrium microemulsion phase. (This could lead to a relatively modest driving force for coarsening and hence, in principle, a long lifetime for the metastable nanoemulsion.) Rather, it is the result of a formulation strategy that stabilizes the system against both Ostwald ripening and coalescence despite a significant driving force for coarsening.

Conclusion

This paper investigates the preparation of nanoemulsions by ultrasonication and their subsequent stability. In the surfactant-rich regime, the droplet diameter decreases exponentially as a function of the input energy density (and, consequently, exponentially in time at fixed power delivery). The saturated size obtained at the end of sonication is governed by the efficiency of the ultrasonic cavitation process in creating high local shear rates and on the characteristic interfacial energy of the droplets. Our data are consistent with the view that the characteristic decay time for the mean droplet size is directly linked to the frequency of bubble collapse events; it is therefore mainly linked to sonication power. The resulting nanoemulsions can be efficiently stabilized against Ostwald ripening by incorporating insoluble species inside the core and/or in the membrane compartment. Compared to conventional emulsions, the small size of the droplets inhibits formation of droplet−droplet contact zones large enough to

(46) Kabalnov, A. *J. Dispersion Sci. Technol.* **2001**, *22*, 1–12.

promote droplet fusion. Therefore, in nanoemulsions, stabilization against coalescence is readily obtained by using enough surfactant in the formulation.

We finally remark that the stability of the herein described nanoemulsions is primarily due to kinetic suppression of the Ostwald and coalescence processes rather than a weak driving force for coarsening caused by proximity to any stable microemulsion domain in the phase diagram. Indeed, we establish that although excess oil could readily be incorporated into a stable microemulsion by sonication, when no trapped species are present the resulting larger droplets are quite unstable. A droplet microemulsion is thus a very particular state, in which swollen micelles have a narrowly defined radius of curvature for which the surfactant layer has very low thermodynamic cost. This allows the entropy of mixing of droplets to stabilize the phase. Deviation from this curvature by adding more oil creates an intrinsically unstable nanoemulsion even for compositions very close in the ternary phase diagram to the thermodynamically stable microemulsion. Unless the oil used is itself insoluble, nanoemulsions can only be made metastable by adding trapped species to either the oil core or the surfactant membrane. This creates an entropic penalty to droplet shrinkage leading to the stability reported above.

Acknowledgment. We thank Nicolas Bremond for useful comments and discussion over the manuscript reviewing process. This work is supported by the Commissariat à l'Energie Atomique et aux Energies Alternatives and the French National Research Agency (ANR) through Carnot funding and Contract ANR-08-PNANO-006-02.

Supporting Information Available: Numerical values of the fitting parameters for the curves of emulsification by sonication. This material is available free of charge via the Internet at http://pubs.acs.org.